ACS APPLIED ENERGY MATERIALS

Article

Cite This: ACS Appl. Energy Mater. 2018, 1, 7046−7051

www.acsaem.org

Enhanced Lithium Transport by Control of Crystal Orientation in Spinel $LiMn_2O_4$ Thin Film Cathodes

Ron Hendriks, Daniel Monteiro Cunha, Deepak Pratap Singh, and Mark Huijben*

MESA+ Institute for Nanotechnology, University of Twente, 7500 AE, Enschede, Netherlands

ABSTRACT: A promising cathode material for rechargeable batteries is $LiMn_2O_4$, which exhibits higher operating voltage, reduced toxicity and lower costs as compared to commonly used $LiCoO_2$ cathodes. However, $LiMn_2O_4$ suffers from limited cycle life, as excessive capacity fading occurs during battery cycling due to dissolution of Mn into the acidic electrolyte. Here, we show that by structural engineering of stable, epitaxial $LiMn_2O_4$ thin films the electrochemical properties can be enhanced as compared to polycrystalline samples. Control of the specific crystal orientation of the $LiMn_2O_4$ thin films resulted in dramatic differences in surface morphology with pyramidal, rooftop or flat features for respectively (100), (110), and (111) orientations. All three types of $LiMn_2O_4$ films expose predominantly ⟨111⟩ crystal facets, which is the lowest energy state surface for this spinel structure. The (100)-oriented $LiMn_2O_4$ films exhibited the highest capacities and (dis)charging rates up to 33C, and good cyclability over a thousand cycles, demonstrating enhanced cycle life without excessive capacity fading as compared to previous polycrystalline studies.

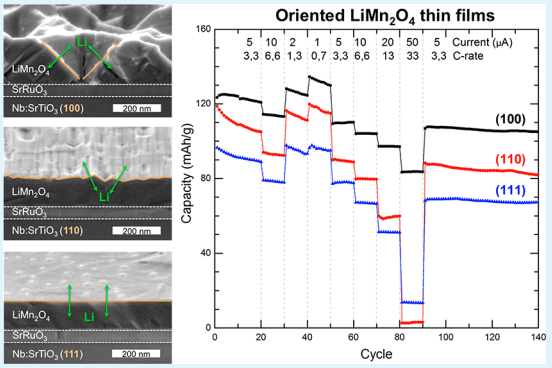

KEYWORDS: *battery cathode, $LiMn_2O_4$, thin films, epitaxy, crystal orientation, spinel, pulsed laser deposition, cycle life*

Since their introduction in the 1990s, lithium-ion batteries have become the main power source for portable electronics and power tools applications. As society transitions toward electric and zero emission mobility, next-generation electric cars require lithium batteries with superior energy and power density, without compromising safety and environmental concerns.[1,2] The cycle life and lifetime are dependent on the nature of the interfaces between the electrodes and electrolyte, whereas safety is a function of the stability of the electrode materials and their interfaces with electrolyte.[3−5] Existing batteries, using conventional layered oxide cathodes, are not only reaching their power and energy density limits, but their application in electric mobility and large applications is also limited by their inadequate cycle life and inherently poor safety features.[6] On the other hand, spinel $LiMn_2O_4$, has emerged as a promising cathode material for next-generation lithium batteries[7,8] because of its relatively high operating voltage (4.1 V vs Li) and comparable energy density (theoretically 148 mAh/g, typical 120 mAh/g) combined with low cost and absence of direct environmental or safety hazards. In spinel $LiMn_2O_4$ (space group $Fd\bar{3}$ m), Li and Mn occupy tetrahedral (8a) and octahedral (16d) sites in the intervening cubic close-packed array of oxygen atoms (32e sites) (Figure 1a). The edge-shared octahedral Mn_2O_4 host framework provides structural stability and interconnects face-shared tetrahedral lithium (8a) sites and empty octahedral (16c) sites (Figure 1b). These interconnected pathways allow the three-dimensional diffusion of lithium ions within the Mn_2O_4 framework, making $LiMn_2O_4$ suitable for high power application. The lithium (de)intercalation at (8a) tetrahedral sites results into the characteristic ∼4 V voltage plateau without distorting the spinel symmetry. Interestingly, this Mn_2O_4 framework can further host lithium into empty octahedral (16c) sites, resulting in a 3 V voltage plateau, almost doubling its capacity (theoretical capacity of $Li_2Mn_2O_4$ is 285 mAh/g) while undergoing a cubic to tetragonal phase transition. Furthermore, the operating voltage of $LiMn_2O_4$ can be increased to ∼5 V by partially substituting Mn with Ni in the Mn_2O_4 framework.[9]

Despite these advantageous properties, $LiMn_2O_4$ cathodes suffer from fading capacity and poor cycle life performance.[10] The origin of this capacity loss was attributed to two factors: first, the onset of Jahn−Teller distortion in deeply discharged electrodes,[1,11,12] and second, the dissolution of Mn ions from the Mn_2O_4 framework.[13] The Jahn−Teller distortion, accompanied by the cubic to tetragonal phase transition, irreversibly damages the structural integrity of the spinel framework during deep cycling down to ∼3 V and causes permanent capacity loss. However, this Jahn−Teller distortion can be avoided by limiting the charging and discharging to the ∼4 V plateau. Whereas, Mn dissolution causing continuous loss of active material and consequently blocking of 3D lithium diffusion pathways, impedes the overall cell performance and remains the key limitation for using $LiMn_2O_4$ cathodes.[2] Previous studies have suggested that acidification of electrolyte, caused

Received: September 2, 2018
Accepted: November 19, 2018
Published: November 19, 2018

DOI: 10.1021/acsaem.8b01477
ACS Appl. Energy Mater. 2018, 1, 7046−7051

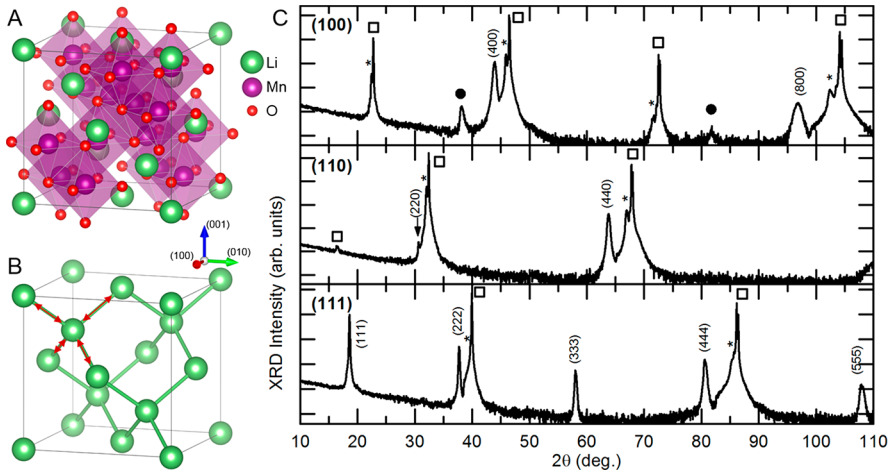

Figure 1. (a) Schematics of the spinel $LiMn_2O_4$ crystal structure, and (b) the structural network for lithium diffusion within the $LiMn_2O_4$ crystal. (c) Out-of-plane XRD measurements of 110 nm $LiMn_2O_4$ epitaxial thin films on 50 nm $SrRuO_3$-coated Nb-$SrTiO_3$ substrates with different crystal orientations: (100), (110), and (111). Nb-$SrTiO_3$ substrate peaks are indicated by □, and $SrRuO_3$ are indicated by *, whereas minor contributions of Mn_2O_3 phase are given by ●.

by reaction of hexafluorophosphate ($LiPF_6$) salt in electrolyte with H_2O, coupled with oxygen loss at the cathode surface, to be the origin of Mn dissolution.[3,4,13] The underlying mechanism can be understood via a disproportional reaction of Mn^{3+} generating soluble Mn^{2+}: $4H^+ + 2Li\,(Mn^{3+}Mn^{4+})O_4 \rightarrow 3\lambda\text{-}Mn^{4+}O_2 + Mn^{2+} + 2Li^+ + 2H_2O$. Various strategies have been suggested to mitigate the Mn dissolution of $LiMn_2O_4$, such as aliovalent doping, surface coating, nanostructuring, mixed phase synthesis.[3,5−10,14−20] Although these strategies have indisputably shown significant enhancement in $LiMn_2O_4$ performance, it remains far from the desired level for usage in applications. Studies have shown that the specific crystal facet in contact with the electrolyte plays an important role in the electrochemical reactions occurring at the cathode surface for single crystalline nanowires,[21] truncated structures[22] and thin films.[23] It was concluded that, as the ⟨111⟩ crystal facet possesses the lowest surface energy and the most dense Mn atom arrangement, it can form a stable solid electrolyte interphase (SEI) layer and mitigate Mn dissolution, thus improving cycling stability. However, the (100)- and (110)-oriented facets were regarded to be better aligned to the lithium diffusion channels, thus able to increase discharge capacities and to facilitate high rate capabilities.[24]

Therefore, perfect control on the interfacial properties between the electrodes and electrolyte is needed but remains a great challenge. Detailed understanding of the electrochemical behavior of specific crystal facets of battery materials can only be obtained when a single type of crystal orientation interfacing the electrolyte can be synthesized. This crucial requirement can be achieved by epitaxial thin film technology, in which the flat surface and restricted lattice plane of the thin film cathode simplify the reaction mechanism at such highly ordered cathode-electrolyte interface. Most studies on $LiMn_2O_4$ thin films have investigated polycrystalline samples, while only limited experimental research has been performed on single crystalline thin films.[23,25−30] Characterization of such epitaxial thin films has previously been focused on the structural properties, and only few reports have shown electrochemical properties by clear redox peaks in the cyclic voltammetry, and discharge capacities of ∼125 mAh/g with clear plateau regions in the charge−discharge curves.[27,29,30] Detailed insight into the relation between the specific crystal orientation toward the adjacent electrolyte and its electrochemical behavior has been lacking, which has hampered the successful development of high-quality $LiMn_2O_4$ cathode with high cyclability. A detailed study by Hirayama et al. concluded from surface X-ray diffraction measurements that a solid-electrolyte interface (SEI) was present on both (111) and (110) surfaces, although the (110) surface was less stable and indicated a higher Mn dissolution.[26] So far the electrochemical performance was only reported for $LiMn_2O_4$ thin films grown on (111)-oriented $SrTiO_3$ substrates,[27,30] where an additional Li_3PO_4 coating was added to prevent a phase transition of the surface region and to suppress Mn dissolution and desorption of oxygen from the surface.

Here, we show that by structural engineering of stable, epitaxial $LiMn_2O_4$ thin films the electrochemical properties can be controlled and enhanced as compared to polycrystalline samples. By changing the crystal orientation of the underlying single crystalline substrate ((100), (110) and (111)) we can control the specific orientation of the $LiMn_2O_4$ thin film and, therefore, the cathode surface toward the adjacent electrolyte. All three types of $LiMn_2O_4$ films exhibit surfaces exposing predominantly ⟨111⟩ crystal facets, the lowest energy state surface for this spinel structure, which results in dramatic differences in surface morphology with pyramidal, rooftop or flat features for respectively (100), (110), and (111) $LiMn_2O_4$ films. Interestingly, the (100)-oriented films exhibited the highest capacities, (dis)charging rates up to 33C, and good cyclability over a thousand cycles, demonstrating enhanced cycle life without excessive capacity fading as compared to polycrystalline studies.[20]

Epitaxial engineering is used in this study to control the crystal orientation of $LiMn_2O_4$ thin films, which enables a unique insight into the relation between electrochemistry and crystal directionality, not obtainable in single crystals or polycrystalline samples. $LiMn_2O_4$ thin films were grown by pulsed laser deposition (PLD) on various single crystal Nb-doped (0.5 wt %) $SrTiO_3$ (Nb:STO) substrates with different crystal orientations ((100), (110) and (111)). All $LiMn_2O_4$ (LMO) thin films were deposited under the same conditions and have a thickness of ∼110 nm. A 50 nm $SrRuO_3$ (SRO)

DOI: 10.1021/acsaem.8b01477
ACS Appl. Energy Mater. 2018, 1, 7046−7051

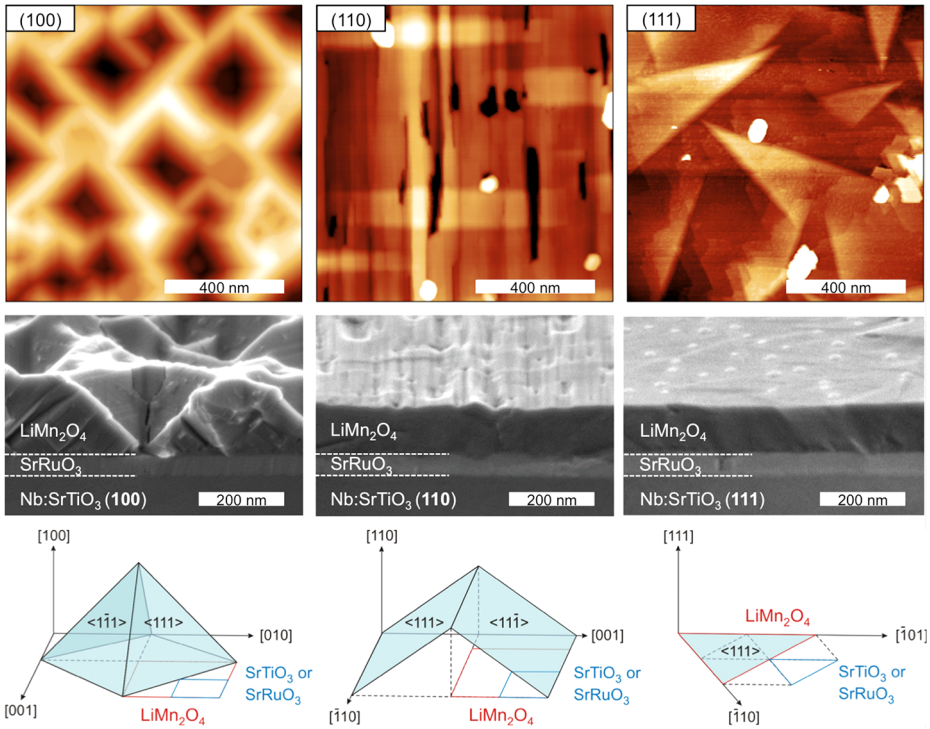

Figure 2. AFM (top) and SEM (middle) analysis of the surface morphology of 110 nm $LiMn_2O_4$ thin films on $SrRuO_3$-coated Nb-$SrTiO_3$ substrates with crystal orientations (100), (110) and (111). SEM images are taken after extensive electrochemical cycling and subsequent cleaning of the surfaces. Schematics (bottom) are shown of the expected crystal facets for the different surface morphologies.

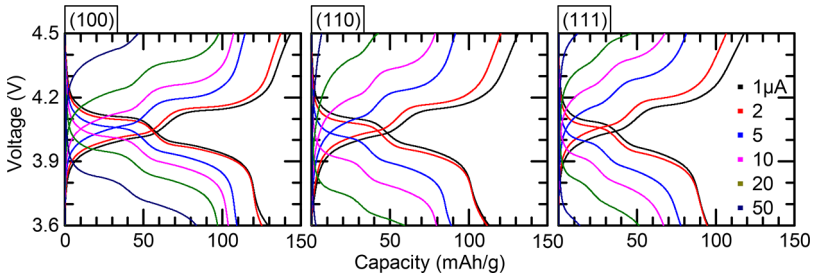

Figure 3. Charge−discharge analysis of 110 nm $LiMn_2O_4$ films with different crystal orientations ((100), (110) and (111)) for various currents (1, 2, 5, 10, 20, and 50 μA). A potentiostatic period of 5 min is used to ensure complete charge or discharge before the next step.

layer was deposited as an intermediate layer to enhance the electrical transport between the LMO cathode and the conducting Nb:STO substrate.[27]

The structural quality of the LMO films was investigated by X-ray diffraction (XRD) analysis, as shown in Figure 1c. The three types of LMO films grown on Nb:STO substrates with different orientations exhibit coherent growth in which the out-of-plane crystal orientation of the films is aligned with the orientation of the substrate. The LMO(111) and LMO(110) films show the presence of highly crystalline epitaxial layers, with a lattice parameter of ∼8.25 Å, without any impurity phase, in good agreement with previous studies of LMO growth on STO(111) and STO(110) substrates.[23,27] This suggests that the PLD process parameters (e.g., temperature, pressure, laser energy density, target composition) were optimized successfully to correct for any loss of volatile lithium during ablation, nucleation or growth. Interestingly, the LMO films with (100)-orientation show minor contributions of a secondary phase, although all three LMO films were grown during the same deposition procedure. The extra peaks suggest the presence of a small amount of Mn_2O_3,[31] which will have a negligible effect on the electrochemical performance of the (100)-oriented $LiMn_2O_4$ thin films, as the anodic reduction and cathodic oxidation reactions in Mn_2O_3 take place below ∼1.3 V.[31,32] This is far below the potential window in our measurements of 3.6−4.5 V. In our case the coexistence of this lithium deficient phase could be due to the enhanced lithium volatility at the (100) surface of $LiMn_2O_4$.[18]

The alignment of the out-of-plane crystal orientation for all types of LMO films, suggests an epitaxial relation between the crystal structures of the deposited LMO films and the underlying Nb:STO substrates, although large differences exist between spinel LMO (a = 8.25 Å) and perovskite STO (a = 3.90 Å). The observed preferred orientation of the LMO films was confirmed by detailed analysis of the in-plane orientation by XRD (not shown) and the surface morphology through atomic force microscopy (AFM), see Figure 2. The surface of the LMO(100) film exhibits square-like structures with significant height differences (RMS ≈ 45 nm), which is in good agreement with previously observed octahedron spinel structures.[22,33] Such pyramidal spinel structures consist of ⟨111⟩ crystal facets on all four sides with an occasional

DOI: 10.1021/acsaem.8b01477
ACS Appl. Energy Mater. 2018, 1, 7046−7051

presence of a truncated top of the pyramid exhibiting a (100) crystal facet. The LMO(110) film forms a layer with rooftop-like structures and a lower surface roughness (RMS ≈ 5 nm), caused by the anisotropic nature of the (110)-plane which favors diffusion of atoms along the $[\bar{1}10]$ direction as compared to the [001] direction.[34] This results in elongated ⟨111⟩ crystal facets exposed on the surface, which are all aligned in the same direction. Finally, the LMO(111) film forms a layer with triangle-like structures exhibiting a very low surface roughness (RMS ≈ 1.5 nm). The triangular shape corresponds to the (111) plane in a cubic structure, for which two different types of in-plane triangle orientations can be observed. Therefore, all three types of LMO films with different out-of-plane orientations ((100), (110) and (111)) exhibit surfaces exposing predominantly ⟨111⟩ crystal facets, which confirms that this is the lowest energy state surface of the spinel crystal structure.[22]

To study the dependence of the lithium transport on the specific crystal orientation of the LMO films, the lithium intercalation characteristics of the LMO thin films were measured by galvanostatic charge−discharge analysis of electrochemical cells against lithium metal with a liquid electrolyte. Figure 3 shows charge−discharge curves for the LMO films with different orientations ((100), (110), and (111)) for various currents, resulting in (dis)charge rates in the range 0.7−33*C*. The characteristic voltage plateaus for these epitaxial LMO thin films are in good agreement with bulk LMO charge−discharge profiles.[7] The total discharge capacity for the slowest rate of 0.7*C* was the highest for the (100)-oriented LMO film (∼129 mAh/g), whereas the (110)- and (111)-oriented LMO films exhibit lower discharge capacities of respectively ∼113 and ∼95 mAh/g. The large surface area of the (100)-oriented LMO film, caused by pyramidal surface morphology, is considered to cause enhanced lithium kinetics as compared to the other crystal orientations. The crystal facets on all films are predominantly ⟨111⟩, which eliminates any possible effect from local variations in crystal facets. The enhanced lithium kinetics for the (100)-oriented LMO films is also demonstrated by the large capacities still achievable during (dis)charging when using higher rates. The used relatively high currents stress the material more and make the variations in lithium intercalation for the different crystal orientations more pronounced. For currents of 20 μA (∼13*C*), the discharge capacities for the (110)- and (111)-oriented films drop to ∼50 mAh/g, whereas the (100)-oriented film still exhibits double the capacity (∼100 mAh/g). The initial drop in discharge capacity after the first charge−discharge cycle may be attributed to anionic reaction occurring at upper voltage cutoff combined with irreversible dissolution of surface lithium and manganese.[16] Furthermore, it is interesting to note that initially at low currents, all films show a slightly higher charge capacity compared to the discharge. Although the exact origin is still unclear, the difference in charge−discharge capacities are within acceptable Coulombic efficiency limits.

The rate dependence of the discharge capacity is shown in more detail in Figure 4 for the LMO films with different crystal orientations. After the initial 20 charge−discharge cycles with 3.3*C* the films are consecutively cycled at various rates in the range 0.7−33*C* before finishing the sequence with the final 40 cycles with 3.3*C*. The results show the stability of the LMO films during substantial cycling, as well as the enhanced performance of the (100)-oriented film as compared to the other orientations. The cycle performance of the (100), (110),

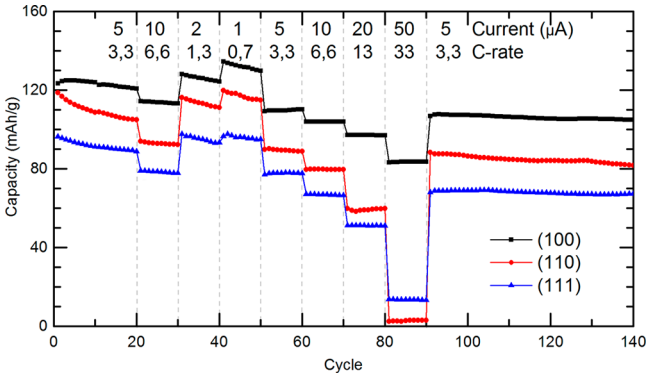

Figure 4. Rate performance analysis of 110 nm $LiMn_2O_4$ thin films on $SrRuO_3$-coated Nb-$SrTiO_3$ substrates with different crystal orientations ((100), (110), and (111)) for various currents, and corresponding *C* rates.

and (111)-oriented LMO thin films was compared after 140 cycles at various C-rates by their discharge capacities of respectively 87, 78, and 76%, as well their Coulombic efficiencies of respectively 97, 94, and 97%. Interestingly, at the highest rate of 33*C*, the (100)-oriented film still exhibits a capacity of about 84 mAh/g, whereas the capacities of the (110)- and (111)-oriented films have been almost reduced to zero. The observed variation in surface area between the differently oriented films (about 50% more surface area for (100)-oriented films as compared to (110)- and (111)-oriented films, see Figure 2), cannot explain this dramatic difference in lithium kinetics. Therefore, it is suggested that the actual difference in lithium intercalation along different crystal orientations within the $LiMn_2O_4$ crystal structure is more pronounced at higher rates when limitations in ionic (lithium) and electric transport become more apparent.

Although the conventional understanding of the Li diffusion in $LiMn_2O_4$ is three-dimensional in which the Li ions hop over the 8a and 16c sites along the interconnected pathways, these zigzagging chains form lithium diffusion channels in specific directions.[35] Previous studies have suggested that although the (111)-oriented facets exhibit the lowest surface energy,[18,36] the (100)- and (110)-oriented facets are better aligned to the lithium diffusion channels, thus increasing discharge capacities and facilitating high rate capabilities.[24] Our results demonstrate that very stable $LiMn_2O_4$ thin films with ⟨111⟩ surface facets exhibit much higher rate capabilities for the (100)-direction as compared to the (110)-direction. Theoretical modeling would provide detailed insight into the diffusion mechanism in which the ease of lithium diffusion through the bottleneck is studied. This oxygen triangle is formed at the contact face between the tetrahedron about 8a and the octahedron about 16c and depends on the displacement of the O atoms, which can vary in differently oriented epitaxial thin films.

The cycle life of such high-performance (100)-oriented LMO films was investigated for several cells during prolonged battery cycling at similar conditions, see Figure 5. The electrochemical behavior of all four cells exhibited good uniformity with initial capacities of about 120−130 mAh/g, which still provided capacities of about 90 mAh/g after a thousand cycles. The stability of the voltage plateaus over the full thousand cycles is shown in Figure 5a, b, and indicates the unchanged internal resistance during the complete prolonged cycling. Figure 5c displays the enhanced cycle life performance for (100)-oriented LMO films with significantly high capacity

DOI: 10.1021/acsaem.8b01477
ACS Appl. Energy Mater. 2018, 1, 7046−7051

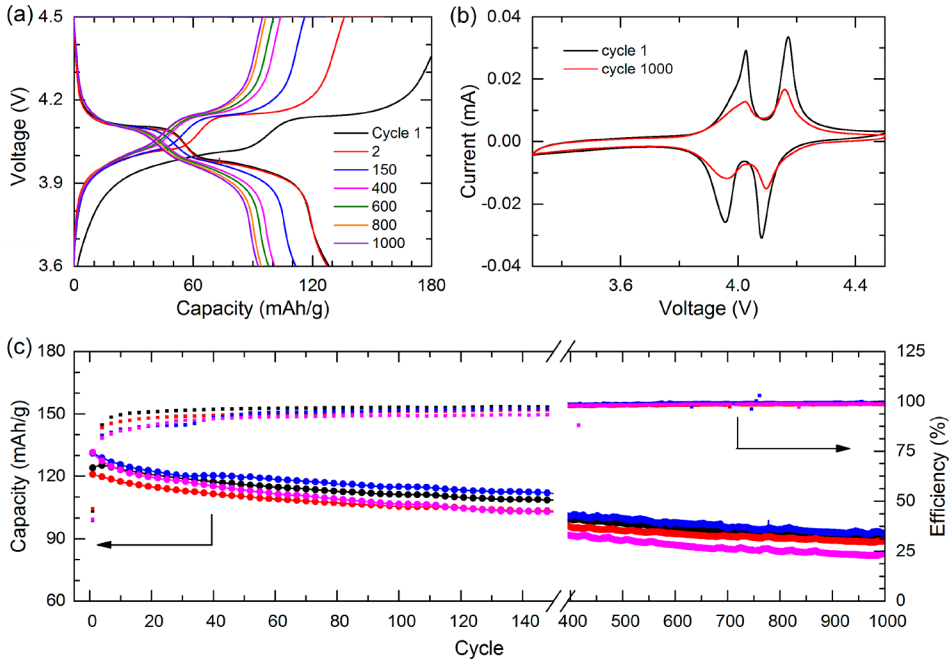

Figure 5. Cycle life analysis of four 110 nm (100)-oriented $LiMn_2O_4$ thin films on $SrRuO_3$-coated Nb-$SrTiO_3$ substrates. The evolution of (a) charge−discharge and (b) cyclic voltammetry behaviors are shown during prolonged cycling. (c) Discharge capacity (circles) and Coulombic efficiency (squares) are given for a thousand cycles. During the measurements a current of 5 μA was used, which provided a (dis)charge rate of 3.3 *C*.

and Coulombic efficiency over thousand cycles as compared to previous studies on bulk and polycrystalline LMO for which the capacity drops below 80% within 50 cycles.[10,20] The very stable cycle performance with very minimal changes in the internal resistance, as can be seen for the (100)-oriented $LiMn_2O_4$ thin films in the constant voltage plateaus in the charge−discharge curves (Figure 5a) and constant peak positions in the cyclic voltammetry (Figure 5b), was confirmed by electrochemical impedance spectroscopy (EIS) experiments during extensive cycling (data not shown).

In conclusion, structural engineering enables improved control over the electrochemical properties of $LiMn_2O_4$ thin films, which is unique for epitaxial thin films and cannot be obtained in single-crystal or polycrystalline samples. Control of the specific crystal orientation of the LMO thin films resulted in dramatic differences in surface morphology with pyramidal, rooftop or flat features for respectively (100), (110) and (111) orientations. All three types of LMO films exhibit surfaces exposing predominantly ⟨111⟩ crystal facets, which is predicted to be the lowest energy crystallographic surface for this spinel structure. The (100)-oriented LMO films exhibited the highest capacities and (dis)charging rates up to 33*C*, and good cyclability over a thousand cycles, demonstrating enhanced cycle life without excessive capacity fading as compared to previous polycrystalline studies.

EXPERIMENTAL METHODS

The $LiMn_2O_4$ and $SrRuO_3$ layers were grown by pulsed laser deposition (PLD) at 600 °C on Nb-doped (0.5 wt %) single crystalline $SrTiO_3$ (100, 110 or 111) substrates from sintered $Li_2Mn_2O_4$ (100 wt % excess Li_2O) and $SrRuO_3$ targets, using a KrF excimer laser operating at 248 nm at a repetition rate of 2 Hz. The Nb-$SrTiO_3$ substrates were annealed at 950 °C for 1.5 h in an oxygen flow of 150 mL/min. The oxygen pressure during growth was 0.13 mbar, while the laser energy fluence was 2.3 J cm^{-2} for the growth of both $LiMn_2O_4$ and $SrRuO_3$. After deposition, the thin films were cooled to room temperature in an oxygen pressure of 0.13 mbar at a rate of 10 °C min^{-1}.

The crystal structure, surface morphology, and thickness of the thin films were investigated by X-ray diffraction (PANalytical X'Pert PRO diffractometer), atomic force microscopy (Bruker ICON Dimension Microscope), and scanning electron microscopy (Zeiss Merlin HR-SEM), respectively.

For electrochemical characterization the films were transferred to an argon atmosphere glovebox (<0.1 ppm of H_2O and O_2) and placed on a hot plate for ∼10 min at 125 °C to remove any water content. Subsequently, they are positioned in an electrochemical EC-ref cell by EL-CELL and combined with a glass fiber separator of 1 mm thickness, 0.6 mL electrolyte with 1 M $LiPF_6$ in 1:1 ethylene carbonate dimethyl carbonate (EC:DMC) and lithium metal anode. The electrochemical measurements were performed at 22 °C using a BioLogic VMP-300 system in a two-electrode setup in which the samples were cycled galvanostatically between 3.6 and 4.5 V with currents of 1, 2, 5, 10, 20, and 50 μA, corresponding to *C* rates of approximately 0.7, 1.3, 3.3, 6.6, 13, and 33*C*, respectively. A potentiostatic period of 5 min is used to ensure complete charge or discharge before the next step.

AUTHOR INFORMATION

Corresponding Author

*Prof. dr. Mark Huijben University of Twente MESA+ Institute for Nanotechnology 7500 AE Enschede, Netherlands e-mail: m.huijben@utwente.nl.

ORCID

Mark Huijben: 0000-0001-8175-6958

Notes

The authors declare no competing financial interest.

ACKNOWLEDGMENTS

T.A.H., D.M.C., D.P.S., and M.H. acknowledge support by The Netherlands Organization for Scientific Research (NWO) under the VIDI grant nr. 13456.

DOI: 10.1021/acsaem.8b01477
ACS Appl. Energy Mater. 2018, 1, 7046−7051

REFERENCES

(1) Dahn, J. R., Ehrlich, G. M. *Handbook of Batteries*, 4 ed.; McGraw Hill: New York, 2011.
(2) Nitta, N.; Wu, F. X.; Lee, J. T.; Yushin, G. Li-ion battery materials: present and future. *Mater. Today* **2015**, *18*, 252−264.
(3) Luntz, A. C.; Voss, J.; Reuter, K. Interfacial challenges in solid-state Li ion batteries. *J. Phys. Chem. Lett.* **2015**, *6*, 4599−604.
(4) Wang, K. X.; Li, X. H.; Chen, J. S. Surface and interface engineering of electrode materials for lithium-ion batteries. *Adv. Mater.* **2015**, *27*, 527−45.
(5) Yuan, Y. F.; Amine, K.; Lu, J.; Shahbazian-Yassar, R. Understanding materials challenges for rechargeable ion batteries with in situ transmission electron microscopy. *Nat. Commun.* **2017**, *8*, 15806.
(6) Lin, F.; Markus, I. M.; Nordlund, D.; Weng, T. C.; Asta, M. D.; Xin, H. L.; Doeff, M. M. Surface reconstruction and chemical evolution of stoichiometric layered cathode materials for lithium-ion batteries. *Nat. Commun.* **2014**, *5*, 3529.
(7) Thackeray, M. M. Manganese oxides for lithium batteries. *Prog. Solid State Chem.* **1997**, *25*, 1−71.
(8) Lee, M. J.; Lee, S.; Oh, P.; Kim, Y.; Cho, J. High performance $LiMn_2O_4$ cathode materials grown with epitaxial layered nanostructure for Li-ion batteries. *Nano Lett.* **2014**, *14*, 993−9.
(9) Ma, J.; Hu, P.; Cui, G. L.; Chen, L. Q. Surface and Interface Issues in Spinel $LiNi_{0.5}Mn_{1.5}O_4$: Insights into a Potential Cathode Material for High Energy Density Lithium Ion Batteries. *Chem. Mater.* **2016**, *28*, 3578−3606.
(10) Gummow, R. J.; de Kock, A.; Thackeray, M. M. Improved capacity retention in rechargeable 4 V lithium/lithium-manganese oxide (spinel) cells. *Solid State Ionics* **1994**, *69*, 59−67.
(11) Van der Ven, A.; Marianetti, C.; Morgan, D.; Ceder, G. Phase transformations and volume changes in spinel $Li_xMn_2O_4$. *Solid State Ionics* **2000**, *135*, 21−32.
(12) Thackeray, M. M.; David, W. I. F.; Bruce, P. G.; Goodenough, J. B. Lithium Insertion into Manganese Spinels. *Mater. Res. Bull.* **1983**, *18*, 461−472.
(13) Hunter, J. C. Preparation of a new crystal form of manganese dioxide: λ-MnO_2. *J. Solid State Chem.* **1981**, *39*, 142−147.
(14) Lee, M. J.; Lho, E.; Bai, P.; Chae, S.; Li, J.; Cho, J. Low-Temperature Carbon Coating of Nanosized $Li_{1.015}Al_{0.06}Mn_{1.925}O_4$ and High-Density Electrode for High-Power Li-Ion Batteries. *Nano Lett.* **2017**, *17*, 3744−3751.
(15) Kim, D. K.; Muralidharan, P.; Lee, H. W.; Ruffo, R.; Yang, Y.; Chan, C. K.; Peng, H.; Huggins, R. A.; Cui, Y. Spinel $LiMn_2O_4$ nanorods as lithium ion battery cathodes. *Nano Lett.* **2008**, *8*, 3948−52.
(16) Bhandari, A.; Bhattacharya, J. Review—Manganese Dissolution from Spinel Cathode: Few Unanswered Questions. *J. Electrochem. Soc.* **2017**, *164*, A106−A127.
(17) Myung, S.-T.; Lee, K.-S.; Kim, D.-W.; Scrosati, B.; Sun, Y.-K. Spherical core-shell $Li[(Li_{0.05}Mn_{0.95})_{0.8}(Ni_{0.25}Mn_{0.75})_{0.2}]_2O_4$ spinels as high performance cathodes for lithium batteries. *Energy Environ. Sci.* **2011**, *4*, 935−939.
(18) Amos, C. D.; Roldan, M. A.; Varela, M.; Goodenough, J. B.; Ferreira, P. J. Revealing the Reconstructed Surface of $Li[Mn_2]O_4$. *Nano Lett.* **2016**, *16*, 2899−906.
(19) Jiao, F.; Bao, J.; Hill, A. H.; Bruce, P. G. Synthesis of ordered mesoporous Li-Mn-O spinel as a positive electrode for rechargeable lithium batteries. *Angew. Chem., Int. Ed.* **2008**, *47*, 9711−6.
(20) Park, S. B.; Shin, H. C.; Lee, W. G.; Cho, W. I.; Jang, H. Improvement of capacity fading resistance of $LiMn_2O_4$ by amphoteric oxides. *J. Power Sources* **2008**, *180*, 597−601.
(21) Hosono, E.; Kudo, T.; Honma, I.; Matsuda, H.; Zhou, H. Synthesis of single crystalline spinel $LiMn_2O_4$ nanowires for a lithium ion battery with high power density. *Nano Lett.* **2009**, *9*, 1045−51.
(22) Kim, J. S.; Kim, K.; Cho, W.; Shin, W. H.; Kanno, R.; Choi, J. W. A truncated manganese spinel cathode for excellent power and lifetime in lithium-ion batteries. *Nano Lett.* **2012**, *12*, 6358−65.
(23) Hirayama, M.; Sonoyama, N.; Ito, M.; Minoura, M.; Mori, D.; Yamada, A.; Tamura, K.; Mizuki, J.; Kanno, R. Characterization of electrode/electrolyte interface with X-ray reflectometry and epitaxial-film $LiMn_2O_4$ electrode. *J. Electrochem. Soc.* **2007**, *154*, A1065−A1072.
(24) Jiang, C.; Tang, Z.; Wang, S.; Zhang, Z. A truncated octahedral spinel $LiMn_2O_4$ as high-performance cathode material for ultrafast and long-life lithium-ion batteries. *J. Power Sources* **2017**, *357*, 144−148.
(25) Sonoyama, N.; Iwase, K.; Takatsuka, H.; Matsumura, T.; Imanishi, N.; Takeda, Y.; Kanno, R. Electrochemistry of $LiMn_2O_4$ epitaxial films deposited on various single crystal substrates. *J. Power Sources* **2009**, *189*, 561−565.
(26) Hirayama, M.; Ido, H.; Kim, K.; Cho, W.; Tamura, K.; Mizuki, J.; Kanno, R. Dynamic structural changes at $LiMn_2O_4$/electrolyte interface during lithium battery reaction. *J. Am. Chem. Soc.* **2010**, *132*, 15268−76.
(27) Suzuki, K.; Kim, K.; Taminato, S.; Hirayama, M.; Kanno, R. Fabrication and electrochemical properties of $LiMn_2O_4/SrRuO_3$ multi-layer epitaxial thin film electrodes. *J. Power Sources* **2013**, *226*, 340−345.
(28) Gao, X.; Ikuhara, Y. H.; Fisher, C. A. J.; Moriwake, H.; Kuwabara, A.; Oki, H.; Kohama, K.; Yoshida, R.; Huang, R.; Ikuhara, Y. Structural Distortion and Compositional Gradients Adjacent to Epitaxial $LiMn_2O_4$ Thin Film Interfaces. *Adv. Mater. Interfaces* **2014**, *1*, 1−10.
(29) Ikuhara, Y. H.; Gao, X.; Huang, R.; Fisher, C. A. J.; Kuwabara, A.; Moriwake, H.; Kohama, K. Epitaxial Growth of $LiMn_2O_4$ Thin Films by Chemical Solution Deposition for Multilayer Lithium-Ion Batteries. *J. Phys. Chem. C* **2014**, *118*, 19540−19547.
(30) Suzuki, K.; Hirayama, M.; Kim, K.; Taminato, S.; Tamura, K.; Son, J. Y.; Mizuki, J.; Kanno, R. Interfacial Analysis of Surface-Coated $LiMn_2O_4$ Epitaxial Thin Film Electrode for Lithium Batteries. *J. Electrochem. Soc.* **2015**, *162*, A7083−A7090.
(31) Xia, H.; Wan, Y. H.; Yan, F.; Lu, L. Manganese oxide thin films prepared by pulsed laser deposition for thin film microbatteries. *Mater. Chem. Phys.* **2014**, *143*, 720−727.
(32) Qiu, Y.; Xu, G.-L.; Yan, K.; Sun, H.; Xiao, J.; Yang, S.; Sun, S.-G.; Jin, L.; Deng, H. Morphology-conserved transformation: synthesis of hierarchical mesoporous nanostructures of Mn_2O_3 and the nanostructural effects on Li-ion insertion/deinsertion properties. *J. Mater. Chem.* **2011**, *21*, 6346−6353.
(33) Wang, F. X.; Wang, X. W.; Chang, Z.; Zhu, Y. S.; Fu, L. J.; Liu, X.; Wu, Y. P. Electrode materials with tailored facets for electrochemical energy storage. *Nanoscale Horiz.* **2016**, *1*, 272−289.
(34) Antczak, G.; Ehrlich, G. Jump processes in surface diffusion. *Surf. Sci. Rep.* **2007**, *62*, 39−61.
(35) Ishizawa, N.; Tateishi, K. Diffusion of Li atoms in $LiMn_2O_4$ − A structural point of view. *J. Ceram. Soc. Jpn.* **2009**, *117*, 6−14.
(36) Kim, S.; Aykol, M.; Wolverton, C. Surface phase diagram and stability of (001) and (111) $LiMn_2O_4$ spinel oxides. *Phys. Rev. B: Condens. Matter Mater. Phys.* **2015**, *92*, 115411.

DOI: 10.1021/acsaem.8b01477
ACS Appl. Energy Mater. 2018, 1, 7046−7051